High-field magnetization process in $R_{1/2}Ca_{1/2}MnO_3$ (R=Sm and Y) up to 100 T

M. Tokunaga
The Institute of Physical and Chemical Research (RIKEN), Wako, Saitama 351-0198, Japan

N. Miura
Institute for Solid State Physics, University of Tokyo, Roppongi, Minato-ku, Tokyo 106-8666, Japan

Y. Tomioka
Joint Research Center for Atom Technology (JRCAT), Tsukuba 305-0046, Japan

Y. Tokura
Joint Research Center for Atom Technology (JRCAT), Tsukuba 305-0046, Japan
and Department of Applied Physics, University of Tokyo, Tokyo 113-0033, Japan
(Received 1 February 1999)

The high-field magnetization process up to 100 T has been studied for manganites with perovskite-type structure $R_{1/2}Ca_{1/2}MnO_3$ (R=Sm and Y). The R=Sm sample showed metamagnetic transitions of the first order at temperatures below 280 K, the R=Y sample showed just monotonous change against magnetic fields. The observed metamagnetic transitions are ascribed to the field-induced collapse of the charge order (a 1/1 ordering of Mn^{3+}/Mn^{4+}). The melting field of the charge order in the R=Sm sample is 50 ± 9 T at 18 K. Together with our previous data for R= Pr and Nd, the present results for R=Sm indicate that reduction of the average ionic radius for the perovskite A site tends to enhance the charge-ordering instability in $R_{1/2}Ca_{1/2}MnO_3$ (R=Pr, Nd, and Sm). [S0163-1829(99)02830-1]

In manganites with perovskite-type structure $R_{1-x}M_xMnO_3$ (R=rare-earth elements and M=Ba, Sr, and Ca), substitution for trivalent R^{3+} with divalent M^{2+} ions produces holes in the system. The doped holes are mobile via hybridized orbitals of Mn $3d$-e_g and O $2p$-σ, and mediate the ferromagnetic double-exchange interaction[1–3] (DE) between localized Mn spins in the t_{2g} states. The change in the valence of the perovskite A site, or the band filling, significantly affects magnetism and conductivity of these manganites.[4,5] Recent investigations have demonstrated that variations in A-site ions play important roles in the magnetic and transport properties of these manganites for a given carrier doping x. Hwang *et al.* showed a direct relationship between the average ionic radius for A-site ions $\langle r_A\rangle$ and the Curie temperature T_C in doped $LaMnO_3$ (Ref. 6) at $x=0.3$. Reduction of the $\langle r_A\rangle$ promotes orthorhombic lattice distortion and reduces the Mn-O-Mn bond angle from 180°. The decrease of T_C with reducing $\langle r_A\rangle$ is attributed to the decrease of the one-electron bandwidth of the e_g electrons.[6,7] Reduction of the $\langle r_A\rangle$ favors the localization of the e_g-orbital carriers, and brings about the reduction of the DE. Then emerges the importance of other interactions that were predominated by DE, such as electron-phonon interaction. These interactions couple degrees of freedom of spin, charge, and lattice (orbital). In manganites with relatively small $\langle r_A\rangle$, such as $La_{1/2}Ca_{1/2}MnO_3$,[4] a 1/1 ordering of Mn^{3+}/Mn^{4+} [charge ordering (CO)] takes place at low temperatures. The CO phenomena have been observed in several transition-metal oxides.[8–11] In manganites, the application of magnetic fields melts the CO (Refs. 7, 12, and 13) due to the coupling among spin, charge, and lattice degrees of freedom. The present work is devoted to extend the study of magnetic-field effects in manganites with relatively small $\langle r_A\rangle$, $R_{1/2}Ca_{1/2}MnO_3$ (R= Sm and Y), utilizing high-pulsed magnetic fields up to 100 T. We measured the isothermal magnetization process of the both manganites at temperatures between 4 K and room temperature. For R=Sm, metamagnetic behavior was observed below the CO transition temperature $T_{CO}\sim280$ K. We ascribed these transitions to the field-induced melting of the CO. Together with our previous results for $R_{1/2}Ca_{1/2}MnO_3$ (R=Pr and Nd),[14] we obtained the relationship between the melting field of the CO and the $\langle r_A\rangle$. Comparison of the melting fields at low temperatures gives direct information of the $\langle r_A\rangle$ dependence of the CO instability. Stoichiometric mixture of Sm_2O_3 (Y_2O_3), $CaCO_3$, and Mn_3O_4 was calcined at 1050 °C (1200 °C). Crystals of $Sm_{1/2}Ca_{1/2}MnO_3$ were synthesized by the floating-zone method.[15] $Y_{1/2}Ca_{1/2}MnO_3$ was also melted in a floating-zone furnace. Both melt-grown samples were ground into powder to suppress the eddy current effect induced in the samples by pulsed fields. Pulsed magnetic fields up to 40 T were generated in a duration time of 8–20 ms utilizing a nondestructive long-pulsed magnet with a 200 or 300 kJ capacitor bank.[16] Magnetization was measured by means of an induction method by employing a couple of pick-up coils that are mounted in a coaxial arrangement.[17] The voltage induced in the pickup coils was recorded by a transient recorder with a sampling time of 5 or 10 μs and integrated numerically to obtain magnetization. Magnetic fields up to 100 T were produced in a duration time of about 7 μs by means of the single-turn technique.[18] Magnetization measurements in short-pulse fields were performed also by

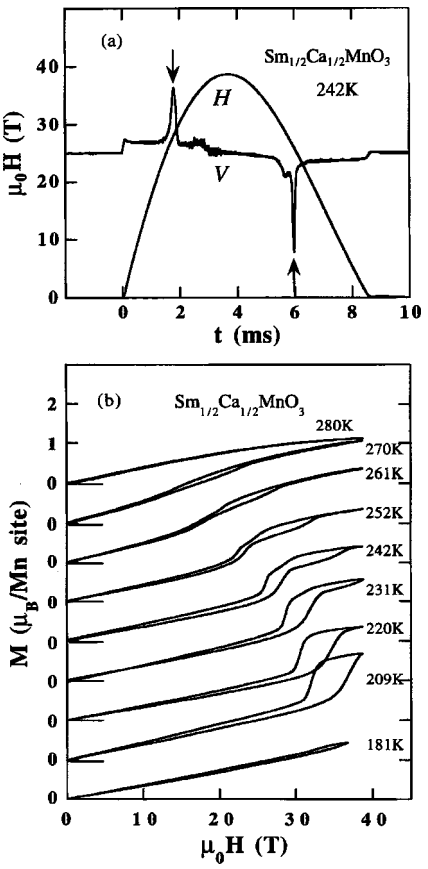

FIG. 1. (a) Magnetic-field (H) profile and induced voltage in the pickup coils (V) as a function of time (t). The metamagnetic transition in the $Sm_{1/2}Ca_{1/2}MnO_3$ appears as the peaks in the V-t curve (see arrows). (b) The M-H curves for $Sm_{1/2}Ca_{1/2}MnO_3$ up to 38 T at various temperatures. Magnetic phase transitions of the first order are observed below 280 K. The transition field increases as the temperature decreases. No manifestations of the transitions are visible below 181 K within the field range up to 38 T.

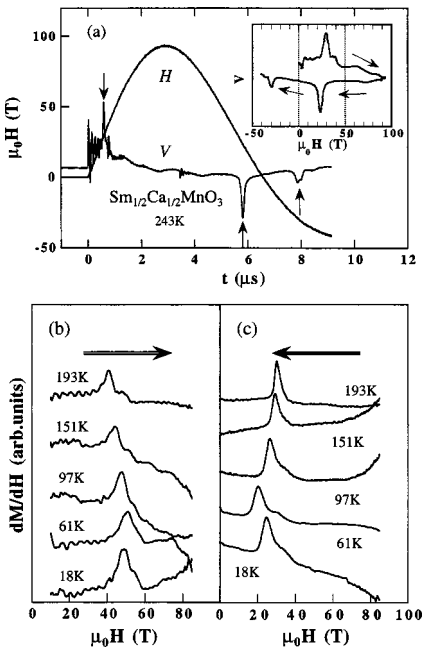

FIG. 2. (a) Line shape of the short-pulse field up to 100 T and the signal induced in pickup coils (V) as a function of time. Three peaks can be recognized for a $Sm_{1/2}Ca_{1/2}MnO_3$ sample at 243 K corresponding to steep changes in magnetization. Magnetic-field dependence of the differential susceptibility dM/dH in (b) field-increasing and (c) -decreasing process. The arrows in (b) and (c) indicate the direction of the field sweep.

means of the induction method.[19] Two oppositely wound five turn coils were connected in series and the sample was inserted in one of the coils. Thus we canceled the component of the external field. Induced voltages in the pickup coils (V), which were in proportion to time derivatives of the magnetization, were recorded by a transient recorder with a sampling time of 5 ns. For the magnetization measurements in short-pulse fields, the powdered sample was dispersed in an epoxy matrix. Figure 1(a) shows a wave form of pulsed field (H) up to 40 T and induced voltage in pickup coils (V) for a powdered $Sm_{1/2}Ca_{1/2}MnO_3$ sample at 242 K as a function of time (t). Since V is in proportion to the time derivative of magnetization, the peak in the V-t curve corresponds to a steep increase or decrease in magnetization. The absolute value of magnetization (M) was evaluated by numerical integration of V. The M-H curves for a $Sm_{1/2}Ca_{1/2}MnO_3$ sample were plotted in Fig. 1(b) for various temperatures from 181 K to 280 K. At 280 K, the M shows only smooth change against the magnetic field. As the temperature decreases below 270 K, where the CO occurs in zero magnetic field,[20] a steep change appears in the slope and hysteresis becomes prominent between the increasing and decreasing field traces. Analogous to $Nd_{1/2}Sr_{1/2}MnO_3$,[12] we ascribe this metamagnetic transition below 280 K to magnetic-field–induced melting of the CO. The transition field increases as the temperature is lowered. Eventually, any manifestation of the transition is no more visible at $T=181$ K within the field range up to 38 T. At temperatures between 231 K and 252 K, a steplike structure was observed in the middle of the transition-field region. Magnetization of $Sm_{1/2}Ca_{1/2}MnO_3$ was measured also in higher fields produced by the single-turn-coil technique. Figure 2(a) shows wave forms of the magnetic field and the signal V from the pick-up coils for a $Sm_{1/2}Ca_{1/2}MnO_3$ sample at $T=243$ K as a function of time. In the case of the single-turn technique, the field is reversed after a half cycle. Thus we can observe a signal in negative magnetic fields up to about 40 T successively after the positive field up to 100 T. Despite the noisy background, we can see three peaks clearly in the V-H curve corresponding to the abrupt changes in the M signal [see arrows in Fig. 2(a)]. The width of the peaks is less than 1 μs. This indicates that the transition is completed in a time scale of μs. The inset of Fig. 2 shows the V as a function of magnetic field. In the first increasing and decreasing field sweeps, the peaks appear at 30 and 23 T, respectively. In the successive field sweep to the negative direction, the peak appears at 30 T, which is the same value as in the increasing field sweep. The difference in the height of the peaks between in the first and the second sweep comes from the difference of the field sweep rate dH/dt. Figures 2(b) and 2(c) show the dM/dH, which are obtained by $(d/dH)\int Vdt$, at various temperatures from 18 K to 193 K in field-increasing and field-decreasing processes, respectively. Figure 3(a) shows the phase boundary of $Sm_{1/2}Ca_{1/2}MnO_3$ on a temperature-magnetic-field plane. Closed and open symbols represent the transition fields in field-increasing and -decreasing processes, respectively. Dif-

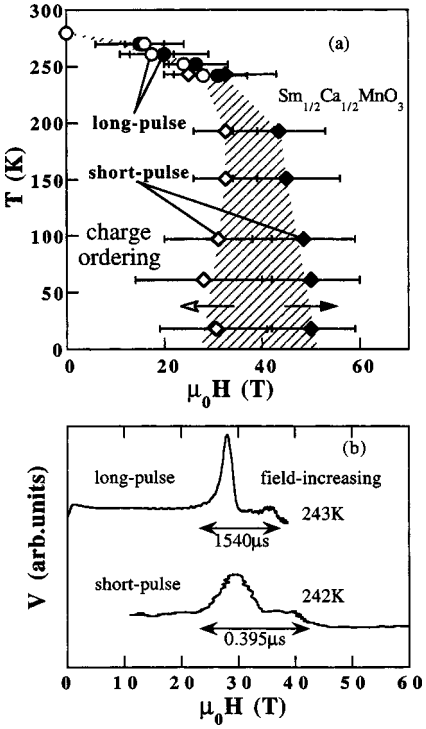

FIG. 3. (a) The phase diagrams of $Sm_{1/2}Ca_{1/2}MnO_3$ in temperature- and magnetic-field plane. Closed and open circles (diamonds) represent the transition fields for the field-increasing and -decreasing process in long- (short-)pulse fields, respectively. The bars represent the peak width of the V-H curve. (b) The V-H at almost the same temperature are compared for short- and long-pulse fields. The peak width of the V-H curve is enhanced in short-pulse fields.

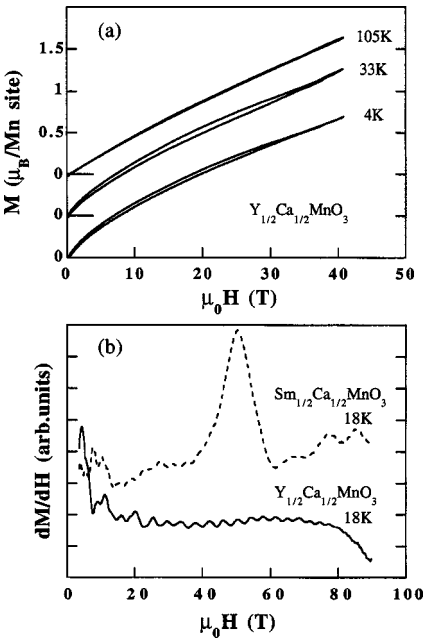

FIG. 4. (a) Magnetization process of $Y_{1/2}Ca_{1/2}MnO_3$ at temperatures 4 K, 33 K, and 105 K. The magnetization increases gradually as the H increases up to 40 T. (b) Magnetic-field dependence of the differential susceptibility dM/dH for $Y_{1/2}Ca_{1/2}MnO_3$ at 18 K. The dM/dH for $Sm_{1/2}Ca_{1/2}MnO_3$ at 18 K is displayed by a dotted line for a comparison.

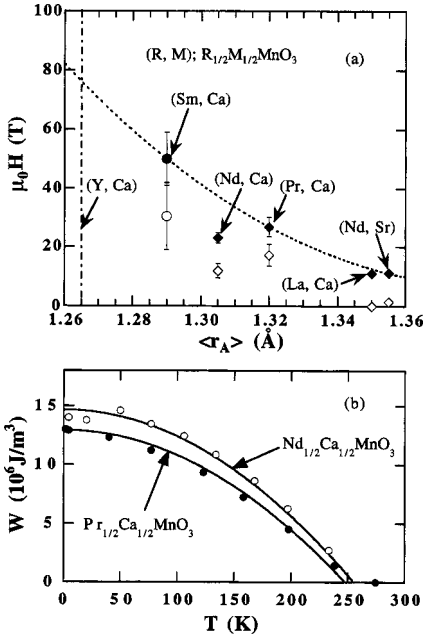

FIG. 5. The transition fields extrapolated to 0 K (H_{C0}) vs the average ionic radius for perovskite A site $\langle r_A \rangle$ for the system $R_{1/2}M_{1/2}MnO_3$, where R is a trivalent rare-earth ion and M is a divalent ion. Open and closed symbols denote the transition fields in the field-increasing and field-decreasing scans. Diamonds and circles are quoted (Refs. 12–14) and present data, respectively. Reduction of the $\langle r_A \rangle$ tends to give rise to the higher transition field. (b) Temperature dependence of the work done by external fields for $Pr_{1/2}Ca_{1/2}MnO_3$ and $Nd_{1/2}Ca_{1/2}MnO_3$ estimated by $W = \int H\, dM$.

ferent symbols in Fig. 3(a), circles and diamonds, distinguish the data points obtained in the long- and short-pulsed fields. It should be noted here that the width of the transition process depends on the field sweep speed. Figure 3(b) shows the induced voltage V in the pickup coils as a function of magnetic field for the field-increasing process in long- and short-pulse fields. In the case of long-pulse fields, it takes 1.54 ms for the field to span from the lower to higher edge of the peak in the V-H curve, while it takes 0.395 μs in the case of short-pulse fields. The difference in profiles of the V-H curves for different scanning speeds indicates that the transition cannot follow such a rapid change of the magnetic field. The transition fields shown in Fig. 3(a) were defined by the average between the lower and higher edge of the peak in the V-H curve. Transition fields in short-pulse fields in the field-increasing (-decreasing) process can be overestimated (underestimated) in magnitude by a few Tesla. The peak width is represented by bars. We can see that the average transition field between the field-increasing and field-decreasing processes increases as temperature decreases similarly to the case of other CO in half-doped $R_{1/2}M_{1/2}MnO_3$.[12–14] Magnetization measurements have been carried out also for a $Y_{1/2}Ca_{1/2}MnO_3$ sample up to 40 T. The M-H curves at temperatures 4 K, 33 K, and 105 K gradually increases up to 40 T [Fig. 4(a)]. Linear extrapolation of the M-H curves at 4 K to higher fields suggests that the magnetization should reach the average spin moment of Mn ions, $3.5\mu_B$ at about $\mu_0 H = 80$ T. In order to check the high-field properties, we have carried out magnetization measurements up to 100 T for a $Y_{1/2}Ca_{1/2}MnO_3$ sample [Fig. 4(b)]. The

data for $Sm_{1/2}Ca_{1/2}MnO_3$ of roughly the same sample amount is also shown in the same scale for a comparison. In contrast to the existence of an evident peak for $Sm_{1/2}Ca_{1/2}MnO_3$ corresponding to a steep increase in magnetization, no clear feature of metamagnetic transition of the first-order nature can be identified in the V-T curve for $Y_{1/2}Ca_{1/2}MnO_3$ up to 100 T. For a series of $R_{1/2}M_{1/2}MnO_3$, the transition fields extrapolated to 0 K (H_{C0}) are plotted in Fig. 5(a) against the average ionic radius for perovskite A site $\langle r_A \rangle$. Here, values for ionic radii were cited from literature.[21] Open and closed symbols denote the transition fields in the field-increasing and -decreasing scans. Diamonds and circles are quoted[12–14] and present data, respectively. In Fig. 5(a), (R, M) denotes $R_{1/2}M_{1/2}MnO_3$. As for $Sm_{1/2}Ca_{1/2}MnO_3$, $Pr_{1/2}Ca_{1/2}MnO_3$ and $Nd_{1/2}Ca_{1/2}MnO_3$, transition fields are defined at the center of the dM/dH peak. The bars in Fig. 5(a) are the width of the transition process [the same as in Fig. 3(a)]. Figure 5(a) demonstrates a clear tendency that a reduction of the $\langle r_A \rangle$ results in the increase of the critical field to destroy the CO. Deviation of the data point for $Nd_{1/2}Ca_{1/2}MnO_3$ from this tendency can be ascribed to the existence of the field-induced Nd moment.[14] The work done by external fields is given by $W = \int H\, dM$. The W for $Pr_{1/2}Ca_{1/2}MnO_3$ and $Nd_{1/2}Ca_{1/2}MnO_3$ until the transition completes is plotted in Fig. 5(b) as a function of temperature. Because of the large saturation moment, the work done to melt the CO for $Nd_{1/2}Ca_{1/2}MnO_3$ is larger than that for $Pr_{1/2}Ca_{1/2}MnO_3$, although the transition field of $Nd_{1/2}Ca_{1/2}MnO_3$ is lower than that of $Pr_{1/2}Ca_{1/2}MnO_3$. This result implies that the field-induced Nd moment interacts with the Mn moment and destabilizes the antiferromagnetic state of the Mn spins. As for the $Y_{1/2}Ca_{1/2}MnO_3$, Arulraj *et al.*[22] reported the existence of the charge-ordered state below 260 K. The present results of magnetization measurements, however, did not show any manifestation of metamagnetic transitions of the strong first-order nature even in a high magnetic field where the manganese spins seemed to be polarized completely. We have studied high-field magnetization processes in half-doped manganites $Sm_{1/2}Ca_{1/2}MnO_3$ and $Y_{1/2}Ca_{1/2}MnO_3$ up to 100 T. $Sm_{1/2}Ca_{1/2}MnO_3$ showed metamagnetic transitions in contrast to $Y_{1/2}Ca_{1/2}MnO_3$, which showed no transition of the strong first-order nature. The metamagnetic transition observed below the charge-ordering temperature is ascribed to be field-induced collapse of the charge ordering. The charge-ordering instability increases as the average ionic radius of perovskite A site $\langle r_A \rangle$ is reduced. For $Nd_{1/2}Ca_{1/2}MnO_3$ that have additional field-induced moments on Nd sites, a deviation is observed from the general trend for the transition field vs $\langle r_A \rangle$.

This work was in part supported by the New Energy and Industrial Technology Development Organization (NEDO), by a Grant-In-Aide for Scientific Research from the Ministry of Education, Science and Culture, Japan, and also by the Special Researchers' Basic Science Program from RIKEN.

[1] C. Zener, Phys. Rev. **81**, 440 (1951).
[2] P. W. Anderson and H. Hasegawa, Phys. Rev. **100**, 675 (1955).
[3] P.-G. de Gennes, Phys. Rev. **118**, 141 (1960).
[4] E. O. Wollan and W. C. Koehler, Phys. Rev. **100**, 545 (1955).
[5] A. Urushibara. Y. Moritomo, T. Arima, A. Asamitsu, G. Kido, and Y. Tokura, Phys. Rev. B **51**, 14 103 (1995).
[6] H. Y. Hwang, S-W. Cheong, P. G. Radaelli, M. Marezio, and B. Batlogg, Phys. Rev. Lett. **75**, 914 (1995).
[7] Y. Tomioka, H. Kuwahara, A. Asamitsu, M. Kasai, and Y. Tokura, Appl. Phys. Lett. **70**, 3609 (1997).
[8] E. J. W. Verwey, P. W. Haaymann, and F. C. Romeijin, J. Chem. Phys. **15**, 181 (1941).
[9] C. H. Chen, S-W. Cheong, and A. S. Cooper, Phys. Rev. Lett. **71**, 2461 (1993); S-W. Cheong, H. Y. Hwang, C. H. Chen, B. Batlogg, L. W. Rupp, Jr., and S. A. Carter, Phys. Rev. B **49**, 7088 (1994).
[10] Y. Moritomo, Y. Tomioka, A. Asamitsu, Y. Tokura, and Y. Matsui, Phys. Rev. B **51**, 3297 (1995).
[11] P. D. Battle, T. C. Gibb, and P. Lightfoot, J. Solid State Chem. **84**, 271 (1990).
[12] H. Kuwahara, Y. Tomioka, A. Asamitsu, Y. Moritomo, and Y. Tokura, Science **270**, 961 (1995); Y. Tokura, H. Kuwahara, Y. Moritomo, Y. Tomioka, and A. Asamitsu, Phys. Rev. Lett. **76**, 3184 (1996); H. Kuwahara, Y. Moritomo, Y. Tomioka, A. Asamitsu, M. Kasai, and Y. Tokura, J. Appl. Phys. **81**, 4954 (1997).
[13] G. Xiao, G. Q. Gong, C. L. Canedy, E. J. McNiff, Jr., and A. Gupta, J. Appl. Phys. **81**, 5324 (1997).
[14] M. Tokunaga, N. Miura, Y. Tomioka, and Y. Tokura, Phys. Rev. B **57**, 5259 (1998).
[15] Y. Tomioka, A. Asamitsu, H. Kuwahara, Y. Moritomo, and Y. Tokura, Phys. Rev. B **53**, 1689 (1996).
[16] S. Takeyama, H. Ochimizu, S. Sasaki, and N. Miura, Meas. Sci. Technol. **3**, 662 (1992).
[17] N. Yamada, S. Takeyama, T. Sakakibara, T. Goto, and N. Miura, Phys. Rev. B **34**, 4121 (1986).
[18] H. P. Furth, M. A. Levine, and R. W. Waniek, Rev. Sci. Instrum. **25**, 949 (1957).
[19] K. Nakao, F. Herlach, T. Goto, S. Takeyama, T. Sakakibara, and N. Miura, J. Phys. E **18**, 1018 (1985).
[20] Y. Tomioka, A. Asamitsu, H. Kuwahara, Y. Moritomo, M. Kasai, R. Kumai, and Y. Tokura (unpublished).
[21] R. D. Shannon, Acta Crystallogr., Sect. A: Cryst. Phys., Diffr., Theor. Gen. Crystallogr. **32**, 751 (1976). The values for XII coordination were used for the ionic radii of perovskite A-site ions.
[22] A. Arulraj, R. Gundakaram, C. N. R. Rao, N. Biswaz Amlan Gayathri, and A. K. Ray-Chaudhri (unpublished).